

CENTER FOR RADAR ASTRONOMY  
Stanford Electronics Laboratories  
Stanford, CA 94305-4055

Explanatory Supplement to the Voyager 1  
Radio Occultation Profiles of Saturn's Rings

by  
Paul A. Rosen

November, 1987

Prepared under  
Jet Propulsion Laboratory contract 953618

## Explanatory Supplement to the Voyager 1 Radio Occultation Profiles of Saturn's Rings

The Voyager 1 Saturn radio occultation experiment of November 13, 1980 provided original data from which profiles of radio optical depth were derived. These profiles have been compiled into six foldout panels which depict graphically many of the important microwave properties of Saturn's rings. This document supplements these profiles. The following paragraphs summarize the principle of radio occultation and the experimental procedure, describe the flow of data from reception on Earth to these final plots, define the quantities plotted, and provide some insight into plotting conventions and possible data interpretations. Papers relevant to the data, covering these aspects in far greater detail, are listed in the *References* section.

### *Radio Occultation Principle*

We define a coherent microwave signal transmitted from the spacecraft as  $E = \sqrt{I_0} \cos \omega t$ . The radiation interacts with ring material causing some of the signal to be scattered and some to be transmitted through the ring coherently, but with altered amplitude and phase. Energy scattered in a narrow cone of angles around the forward direction is received on Earth. The scattered signal is not represented in the accompanying profiles. [See Tyler (1987) for a summary of the Voyager Radio Science experiment and a discussion of the scattered signal.] The coherent component is diffracted by the rings and propagates through free space toward Earth, where it is received. The received signal will have the form  $E_{\text{rec}} = \sqrt{I_{\text{rec}}} \cos(\omega t - \phi_{\text{rec}})$ , where  $\sqrt{I_{\text{rec}}(t)}$  and  $\phi_{\text{rec}}(t)$  are the time-dependent amplitude and phase of the signal. They reflect changes to the spacecraft-generated signal due to ring material and diffraction effects as well as frequency drift due to motion-induced Doppler shift and plasma interaction. Both the

Doppler and the diffraction effects can be modelled and removed. The plasma effects are small. In phasor notation,  $E_{\text{rec}} = \sqrt{I_{\text{rec}}} \exp(-i\phi_{\text{rec}})$ .

### *Signal Processing for Voyager 1 at Saturn*

For Voyager 1 at Saturn, two signals of different frequency were transmitted and received simultaneously, with wavelengths  $\lambda$  of approximately 3.6 and 13 cm. Both signals were derived from a common source, the Ultra-Stable Oscillator (USO), on-board the spacecraft such that  $\lambda(3.6 \text{ cm}) \equiv 3\lambda(13 \text{ cm})/11$  regardless of the USO's frequency stability. The USO was stable on the order of one cycle of phase drift over 100 seconds at  $\lambda = 3.6 \text{ cm}$ .

The center frequency of the receivers was controlled by computer (Programmable Oscillator Control Assembly, or POCA) to ensure that the drifting signal would remain in the passband. Heterodyning and filtering occurred at successive bandwidths of 300 MHz and 10 MHz, after which the 3.6 (13) cm signal was filtered to 150 (50) kHz bandwidth, mixed to baseband, sampled and stored on computer compatible tapes.

Figure 1 illustrates the subsequent processing steps carried out at Stanford Center for Radar Astronomy. Data at both wavelengths were processed in the same way. The characteristics of the signal at the output of a processing stage are represented graphically by small cartoons of the phase and/or the spectrum located nearby. The raw data were filtered and decimated to reduce the data volume. No ring related information is lost in this process. Knowledge of the motion of the spacecraft, Saturn, and Earth was supplied by the Voyager Navigation Team in the form of a Celestial Reference System (CRS) tape, which allowed reconstruction of the expected Doppler shift. The POCA steering offsets combine with the Doppler estimates to give the expected location of the signal frequency in the passband. This location is described by a set of polynomial coefficients indexed by

time. Digital mixing was applied to the data using these coefficients to shift the signal to the center of the passband (first order steering). Residual frequency drifts were removed empirically by filtering the data further and modelling the large time-scale frequency changes still present in the data. A new set of coefficients was generated for second-order steering.

The time of an event in the data can be mapped to a spatial position in the rings, through the same geometric reconstruction used to obtain Doppler shifts. The data were filtered and decimated to a time resolution which corresponds to a chosen spatial resolution in the ring plane. The samples were then interpolated to be uniformly spaced in radius from Saturn. At this point the data represent a spatial profile of the rings. Because the coherent signal was diffracted by the rings, the spatial resolution of ring features at this stage of processing was poor ( $\sim 15$  km at 3.6 cm). Diffraction reconstruction, a matched filter technique modelled from the physical diffraction process, was performed on the data to improve the resolution to 400–5000 m. The resulting data are denoted by the phasor  $\hat{E} = \sqrt{\hat{I}} \exp(-i\hat{\phi})$ .

#### *Derived quantities*

The quantities plotted in these profiles are derived from  $\hat{I}$  and  $\hat{\phi}$ . Radio optical depth is a logarithmic measure of radio signal attenuation.<sup>1</sup>

---

<sup>1</sup>We use the term “optical depth” for all wavelengths, as mandated by its mathematical definition. Modern radar experiments have rendered the term somewhat parochial, however. Recent papers from SCRA have attempted to avoid the awkward juxtaposition of “radio” and “optical” by using the term “radio opacity” instead of “radio optical depth”. The latter is used for these profiles, mostly for consistency with terminology of occultation observations at other wavelengths. However, these terms are identical in definition.

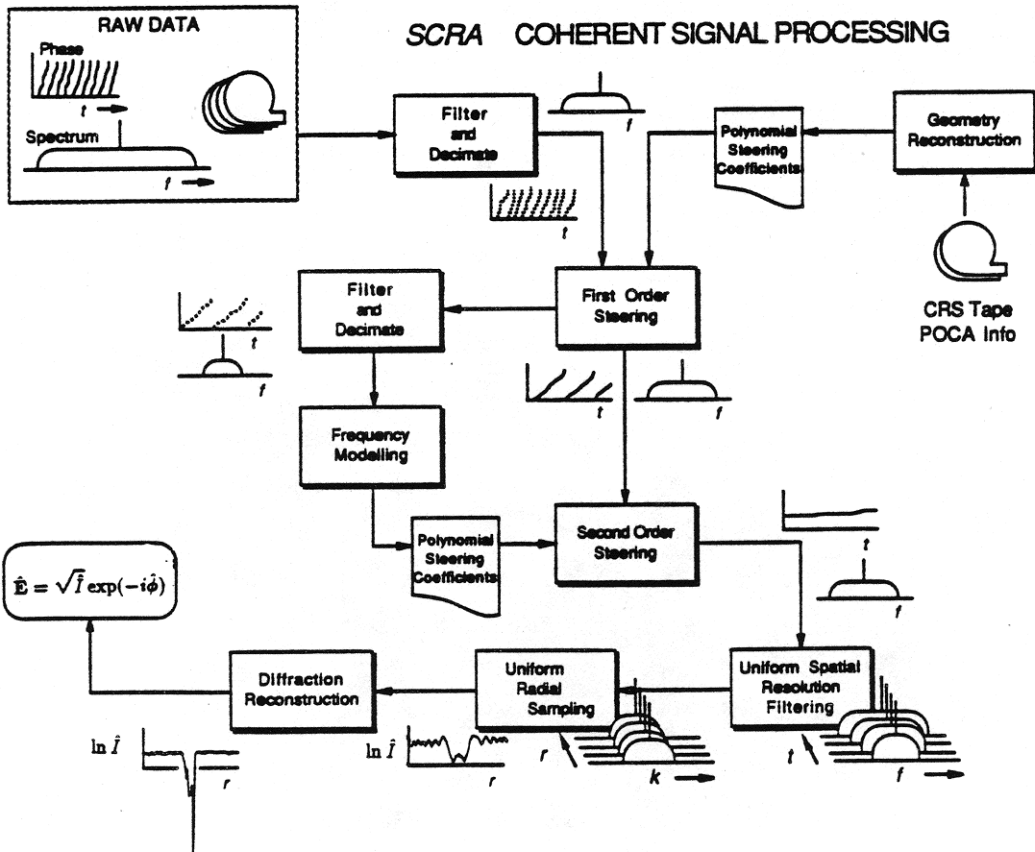


Figure 1: Summary of data processing steps necessary to obtain the accompanying diffraction corrected profiles.

Normal radio optical depth is defined

$$\tau(r, \lambda) = -\mu_0 \ln [\hat{I}(r, \lambda)/I_0(\lambda)] \quad (1)$$

where  $\lambda$  is the wavelength of the transmitted signal, in this case either 3.6 or 13 cm,  $r$  is the radial location, and  $\mu_0$  is  $\sin B$  where  $B$  is the ring opening angle. Observations of dispersive optical depth and phase shift (see below) provide powerful measures of centimeter to meter sized particles.

Differential optical depth is defined

$$\Delta\tau(r) = \tau(r, 3.6 \text{ cm}) - \tau(r, 13 \text{ cm}). \quad (2)$$

Positive  $\Delta\tau$  generally indicates the presence of cm-sized particles. Also, generally  $a \gg \lambda$  if  $\Delta\tau = 0$  and  $\tau \neq 0$ .

Differential phase is defined:

$$\Delta\phi(r) = \hat{\phi}(r, 13 \text{ cm}) - \frac{3}{11}\hat{\phi}(r, 3.6 \text{ cm}) \quad (3)$$

and is measured in cycles at 13 cm  $\lambda$  rather than radians. Generally,  $\Delta\phi > 0$  for  $\lambda$ -sized or smaller particles,  $\Delta\phi \rightarrow 0$  for  $a \gg \lambda$ , and  $\Delta\phi < 0$  implies presence of charged particles.

The actual scattering properties of rings are considerably more complex than the simple interpretations given above. Thus exceptions to this description are prevalent in the data.

Each of the plotted profiles included here displays measurements of Eqs. (1), (2), and (3), where normal radio optical depth  $\tau(r, \lambda)$  is given for  $\lambda = 3.6$  cm. Optical depth is plotted over the range  $-0.1$  to  $+1.6$  with  $\tau = 0$  denoting the free space value. Positive optical depth indicates presence of ring material, and is plotted DOWNWARD. Measurement of high material density is obtained only by sacrificing spatial resolution. Gray shading denotes confidence;  $\tau \sim 1$  represents the maximum reliable estimate at useful resolutions.

Differential optical depth and differential phase are plotted on scales  $-0.4$  to  $+0.8$  and  $-0.75$  to  $+0.75$ , respectively, with positive DOWNWARD. Long range drift in differential phase could be due to plasma effects or long-term drift in radio instrumentation. Phase discontinuities are artifacts of modulo  $360^\circ$  operation at either 3.6 cm or 13 cm. These curves should be interpreted only in close conjunction with optical depth and differential optical depth measurements.

#### *Detail on Plot Characteristics*

A number of plotting features warrant attention.

1. Optical depth, plotted as the solid curve in the uppermost frame of each panel, increases downward. Since  $\tau$  is a measure of signal attenuation, its increase corresponds to a decrease in signal level. As the signal level decreases, it becomes less distinguishable from the thermal noise. It is therefore natural to situate higher confidence data — lower  $\tau$  — more prominently on the page. Differential  $\tau$  is plotted in the same fashion in the center frame of each panel.
2. Gray shading represents confidence intervals for the optical depth along the solid curve. The true value of  $\tau$  lies within the shaded region with 70 percent probability. This corresponds roughly with the conventional notion of “one-sigma error bars”. Non-uniformity in the density of the gray is a plotting artifact and carries no significance.
3. Differential phase is *plotted* in the same sense as  $\Delta\tau$  (increasing downward). By *computing*  $\Delta\phi$  in the opposite sense from  $\Delta\tau$ , both differential measurements will fluctuate roughly in concert under the influence of changing particle sizes. Confidence intervals for  $\Delta\phi$  are difficult to realize graphically and are therefore

omitted. The optical depth confidence provides a measure of the reliability of the phase. Long-range phase drift could be due to plasma effects or drift in radio instrumentation. Interpretation of long-range effects with regard to ring properties should be made with extreme caution.

4. The plot of  $\Delta\phi$  is occasionally discontinuous. The true phase of the signal is continuous. However, computing its value from the components of the complex signal  $\hat{E}$  leads to a modulo one-cycle ambiguity ( $-\frac{1}{2} < \hat{\phi} \leq \frac{1}{2}$ ). From the definition of  $\Delta\phi$ , if

$$\begin{aligned}\hat{\phi}(r + dr, 13 \text{ cm}) &= \hat{\phi}(r, 13 \text{ cm}) \pm 1 \\ \hat{\phi}(r + dr, 3.6 \text{ cm}) &= \hat{\phi}(r, 3.6 \text{ cm}),\end{aligned}$$

then

$$\Delta\phi(r + dr) = \Delta\phi(r) \pm 1.$$

Similarly, if

$$\begin{aligned}\hat{\phi}(r + dr, 3.6 \text{ cm}) &= \hat{\phi}(r, 3.6 \text{ cm}) \pm 1 \\ \hat{\phi}(r + dr, 13 \text{ cm}) &= \hat{\phi}(r, 13 \text{ cm}),\end{aligned}$$

then

$$\Delta\phi(r + dr) = \Delta\phi(r) \mp 3/11.$$

Thus discontinuities in the computed values of  $\hat{\phi}$  can lead to discontinuities in the plots. No attempt has been made to “unwrap” the phase.

5. The resolution of the profiles varies from one region to another to optimize the trade-off between signal-to-noise ratio and resolution. The profiles were derived from diffraction-reconstructed data sets with intrinsic resolutions of 400 m, 1000 m, 5000 m, and sample spacings of 200 m, 500 m, and 2500 m respectively.

Where coarser resolution was required coherent box-car averaging was used:

$$\langle \hat{E}(r_i) \rangle = \frac{1}{N} \sum_{k=i-N/2}^{k=i+N/2-1} E(r_k).$$

For complex data with Gaussian real and imaginary noise components,  $\langle \hat{E} \rangle$  is the minimum variance unbiased estimator of the signal. All profiles in Ring C are plotted at 2.5 km resolution. The Cassini division is plotted at 4.5 km resolution, but has roughly the same noise level as Ring C. Ring A and Ring B have a variety of resolutions, chosen to emphasize particular features present in the data. All resolutions are indicated on the plots except for the insets. All insets *except* for Ring B have 400 m resolution. The Ring B inset has 5 km resolution.

6. There are a number of locations where no data are plotted. There are three reasons this may occur.
  - (a) Resolution change. In this case, a vertical line is drawn at the boundary between two regions of different data resolution. Some small portion of the data is removed around this to emphasize the transition.
  - (b) Data loss. In one region in the Cassini division (119000–119150 km) some phase information was lost during data acquisition. The diffraction reconstruction exacerbated the problem by spreading its influence over 150 km. To avoid possible over-interpretation, these data are removed.
  - (c) Misleading information. Some of the coarse resolution data cause sharp radial transitions of  $\Delta\tau$  or  $\Delta\phi$  to appear to be smeared over large ranges. Then the finer resolution profile of  $\tau(3.6 \text{ cm})$  appears inconsistent with the correspond-

ing differential measurements. Blanking these regions indicates that no meaningful differential information exists for these data at the given resolution.

7. Horizontal and vertical scales were chosen to be as consistent as possible from one panel to another. The radial scale of all profiles *except* Ring B is 100 km:1 cm (10000000:1). Ring B, due to overwhelming noise and consequent poor resolution, is plotted at 500 km:1 cm. All insets *except* the Ring B inset focussing on the co-orbital 2:1 resonance (see item 8 below) are plotted at 10 km:1 cm. The Ring B inset is 100 km:1 cm.

Vertical scales for  $\tau$ ,  $\Delta\tau$ , and  $\Delta\phi$  are consistent among all panels. Ring B uses the same scale for  $\tau$ , but establishes a different zero- $\tau$  level to accommodate its higher optical thickness. All insets expand the  $\tau$  scale by a factor of 2.

The scaling differences between Ring B and the other profiles are significant. Ring B is not directly comparable to the other rings. Therefore for emphasis, its profile has been removed from its proper spatial position between Ring C and the Cassini division and placed after Ring F on the panels.

8. Between the  $\tau$  and  $\Delta\tau$  profiles small vertical lines occasionally stem down from the horizontal  $\tau$  axis, accompanied by letter/number codes. These markings represent locations where ring particles are in resonance with a satellite orbiting outside the ring system, as computed by Lissauer and Cuzzi (1982). To be in resonance, a particle must orbit the planet  $n$  times for every  $m$  revolutions of the satellite. Here  $n$  and  $m$  are integers. Resonances drive many important phenomena in Saturn's rings, e.g. the regular oscillations of  $\tau$  present in the Ring A profiles. The name of the satellite causing the resonance and the ratio

$n:m$  are coded into the label which is aligned slightly to the right of the resonance location marker. The labels are displaced vertically to avoid overlap of those closely spaced. For example, at 136804 km, the ring particles orbit 36 times for every 35 orbits of the satellite Prometheus. Thus the label associated with the marker at 136804 km is "PRO 36:35". Table 1 lists the abbreviations for the Saturnian satellites involved in resonant interactions along with their names and semimajor axes.

9. Miscellaneous plotting conventions:

- (a) The zero-level for each curve is shown through the entire extent of a profile by a dashed line. In Ring B, the dashed line for  $\tau(r, 3.6 \text{ cm})$  resides above the grid and the plot title.
- (b) The plot titles were chosen as reference names of the region on a panel and do not conform to any standard nomenclature. For example, "Central Ring C" is not completely centered; however, it is central to the other two Ring C plots.
- (c) The vertical axes are numbered but lack solid lines, except at the start of Ring C, the end of Ring F, and around Ring B. This is designed to give the sense of continuity among the panels which represent one very large ring system. Absence of vertical lines also facilitates aesthetic concatenation of the panels. Ring B is delimited by lines to reinforce the fact that the scales are quite different.

10. Q.O.P. The principle of radio occultation is conceptually simple, yet its application to planetary systems uncovers their vast beauty and complexity in rigorous, quantitative detail. The Stanford Center for Radar Astronomy has adopted as its dic-

Code	Satellite	$a_s$ (km) <sup>†</sup>
PRO	Prometheus	139,849
PAN	Pandora	142,249
EPI	Epimetheus	151,966
JAN	Janus	152,021
MIM	Mimas	185,970
ENC	Enceladus	238,347
TIT	Titan	1,221,910
HYP	Hyperion	1,484,230
IAP	Iapetus	3,558,430

† Satellite semimajor axis  
from JPL NAIF ephemeris  
at epoch 11/13/80 3:25:55 UT

Table 1: List of satellites of Saturn, by code name, involved in resonant interactions with ring particles.

tum an aphorism which concisely expresses this principle for radio as well as stellar sources:

*Quod Occultum Patefaciet*

or

That which is hidden shall reveal

The use of the future tense emphasizes the continuing relevance of this technique to present and future planetary studies.

Computer tapes of similar profiles, each generated at *constant* resolution, are available from the National Space Science Data Center, Greenbelt, MD. Both pre- and post- diffraction reconstruction data are included on the tapes. Sufficient geometric information is provided to allow independent reproduction of the diffraction corrected results. Data sets of 4200 m and 900 m resolution are on file. Both sets have the same title and are distinguished by their resolution and date of submission to the NSSDC. The title is "X- and S-band Opacity and Phase Profile of the Rings of Saturn". Here X-band (S-band) refers to the 3.6 cm (13 cm) data. Opacity is synonymous with optical depth. The 4200 m resolution profiles were submitted June 21, 1984; the 900 m profiles were submitted March 20, 1986. In addition, 400 m resolution profiles will be available in early 1988. These represent the finest possible resolution at which the entire ring profile can reliably be reconstructed.

#### *Acknowledgements*

The following people participated in the Voyager 1 Saturn radio experiment and helped to bring the data to their present state. EAM, RAS and GLT have provided particularly helpful comments and suggestions during the production of these profiles and documentation.

G.L. Tyler, Principal Investigator  
V.R. Eshleman  
E.A. Marouf  
R.A. Simpson  
D.N. Sweetnam (JPL)  
H.A. Zebker  
The Radio Science Support Team (JPL)

### *References*

Papers discussing the pertinent theory of radio occultation:

ESHLEMAN, V.R., G.L. TYLER, J.D. ANDERSON, G. FJELDBO, G.S. LEVY, G.E. WOOD, AND T.A. CROFT (1977). Radio science investigations with Voyager. *Space Sci. Rev.* 21, 207-232.

MAROUF, E.A. (1975). *The Rings of Saturn: Analysis of a Bistatic Radar Experiment*. Ph.D. dissertation, Stanford University, Stanford, Calif.

MAROUF, E.A., G.L. TYLER, AND V.R. ESHLEMAN (1982). Theory of radio occultation by Saturn's rings. *Icarus* 49, 161-193.

Papers discussing signal processing techniques and some data analysis:

MAROUF, E.A., G.L. TYLER, AND P.A. ROSEN (1986). Profiling Saturn's rings by radio occultation. *Icarus* 68, 120-166.

MAROUF, E.A., G.L. TYLER, H.A. ZEBKER, R.A. SIMPSON, AND V.R. ESHLEMAN (1983). Particle-size distribution of Saturn's rings features from Voyager 1 radio occultation. *Icarus* 54, 189-211.

ROSEN, P.A. (1985). *Processing with the Fresnel Transform: Applications to Inverting Diffraction-limited Data from the Voyager 1 Radio Occultation Experiment*. Technical Report No. D840-1985-

1. Center for Radar Astronomy, Stanford Electronics Laboratories,  
Stanford, Calif.

TYLER, G.L., E.A. MAROUF, R.A. SIMPSON, H.A. ZEBKER, AND  
V.R. ESHLEMAN (1983). The microwave opacity of Saturn's rings at  
wavelengths of 3.6 and 13 cm from Voyager 1 radio occultation. *Icarus*  
54, 160-188.

An overview of the Voyager Radio Science experiment is given in:

TYLER, G.L. (1987). Radio propagation experiments in the outer  
Solar System with Voyager. *Proc. IEEE*, October issue.

Paper giving theoretical locations of strong satellite resonances:

LISSAUER, J.J. AND J.N. CUZZI (1982). Resonances in Saturn's  
Rings. *Astron. J.* 87(7), 1051-1058.

This document and the accompanying profiles were prepared by  
Paul A. Rosen of the Stanford Center for Radar Astronomy as part of  
a Ph.D. dissertation (in preparation, 1987). Please direct comments  
and/or questions to:

Paul A. Rosen (415) 723 3597 (through 6/88) or  
G. Leonard Tyler (415) 723 3535  
Stanford Center for Radar Astronomy  
Stanford Electronics Laboratories  
Durand Building 232  
Stanford, CA 94305-4055